Verifying Theoretical Models of Flux Pinning Using Heavy Ion Irradiated YBCO Thin Films

P. Paturi, M. M. Aye, A. Soman, C. Notthoff, P. Kluth, N. Strickland, and H. Huhtinen

***Abstract*—We have irradiated $YBa_2Cu_3O_{6+x}$ (YBCO) films without artificial pinning sites with Ag^+ ions with energies of 75 MeV and 150 MeV and fluences between 2–8·10^{11} ions/cm^2 in order to create as controlled nanorod pinning sites as possible. The structural and superconducting properties were determined before and after the irradiation with x-ray diffraction and magnetic measurement. After the irradiation also transport and transmission electron microscopy measurements were made. It was noted that the ion tracks are all parallel to the YBCO*c*-axis of the sample and those done with 150 MeV ions formed continuous 5 nm diameter tracks, whereas with 75 MeV ions, the tracks were not continuous through the sample. The T_c and $J_c(0\,T)$ decreased with the irradiation, but the in-field J_c increased. The maximum increase was obtained with the 150 MeV and 4·10^{11} ions/cm^2 sample with continuous rods, where the distance between the rods was closest to the diameter of the rods. Thus, the previous theoretical models predicting optimal pinning when the pinning site diameter is approximately equal to the distance between the pinning sites, are experimentally verified for these very pure samples, with no other external pinning sites.**

***Index Terms*—Flux pinning, heavy ion irradiation, theoretical models, thin films, YBCO.**

I. Introduction

APPLICATIONS of high-temperature superconductivity (HTS) are finally becoming a reality. $YBa_2Cu_3O_{6+x}$ (YBCO) wires are now being produced industrially in kilometer lengths with remarkable properties [1]. Advances in nanotechnology has enabled the use of YBCO wires at high magnetic fields. Without tailored nanometer-scale non-superconducting inclusions, i.e., artificial pinning centers (APCs), the usable magnetic field range of these wires would be orders of magnitude smaller [2], [3]. This is because flux pinning defines the critical current density, J_c, at high fields. Without the nanoscopic pinning sites, the magnetic vortices move due to the Lorentz force, leading to observable voltages and the loss of superconductivity. On the other hand, too high a concentration of pinning sites leads to a smaller superconducting cross-section, lowering the critical current, I_c. Thus, there is an optimal pinning site concentration for each field and temperature.

Using analytical pinning models [4], [5], [6], [7] and a machine learning model [8], [9], we have previously predicted that at low temperature and high field the maximum J_c is found when the average distance between the pinning sites is roughly equal to the diameter of the pinning sites. On the other hand, the optimal pinning site diameter is around 8–10 nm [10], so that each pinning site is strong enough to break the vortex-vortex forces in the vortex lattice, but uses as small a volume of the matrix as possible. This type of single vortex pinning leads to very small α values in the magnetic field dependence of $J_c \propto B^{-\alpha}$, and thus smaller degradation of J_c with magnetic field [11].

Typically, the best APCs are considered to be non-superconducting rods of e.g., BaM O_3 (M = Zr, Sn, Hf. . .) due to their similar geometry with the vortices [12], [13], [14], [15]. If the YBCO is grown with pulsed laser deposition (PLD), the rods are self-assembled during growth [16], but they typically cause a large number of defects and strain around them [17]. Since the excess strain and defects reduce the quality of the YBCO matrix, the critical current at self-field, J_{c0} [4] is also reduced, which lowers the overall J_c of the samples. Therefore, these samples are not optimal for testing the theoretical models. Instead, samples with c-oriented pinning sites with minimal degradation of the YBCO matrix would be needed. These can be obtained by heavy-ion irradiation [18].

In this work, we have irradiated a set of APC-free YBCO films with heavy ions in order to create APCs which disturb the YBCO matrix as little as possible. We have then investigated the structural and superconducting properties of these samples in great detail to compare them to the predictions of the theoretical models.

II. Experimental

YBCO thin films were grown on (100) single crystal $SrTiO_3$ substrates using pulsed laser deposition with a XeCl excimer laser (λ = 308 nm), 750 °C substrate temperature and flowing oxygen. After deposition, the films were subjected to atmospheric oxygen treatment for 10 min at 700°C. More details of the deposition are given in [19], [20]. All the films were deposited in the same conditions and from the same large grained target made with the solid state method. Immediately after deposition the magnetic properties were measured magnetically

Received 17 September 2024; revised 10 December 2024 and 3 January 2025; accepted 4 January 2025. Date of publication 10 January 2025; date of current version 21 January 2025. This work was supported in part by the Jenny and Antti Wihuri Foundation and in part by the Royal Society of New Zealand under Marsden Fund under Grant VUW1805. *(Corresponding author: P. Paturi.)*

P. Paturi, M. M. Aye, and H. Huhtinen are with the Wihuri Physical Laboratory, Department of Physics and Astronomy, University of Turku, 20014 Turku, Finland (e-mail: petriina.paturi@utu.fi).

A. Soman and N. Strickland are with the Victoria University of Wellington, Kelburn 6012, New Zealand.

C. Notthoff and P. Kluth are with the Research School of Physics, Australian National University, Canberra, ACT 2601, Australia.

Color versions of one or more figures in this article are available at https://doi.org/10.1109/TASC.2025.3527949.

Digital Object Identifier 10.1109/TASC.2025.3527949

with a Physical Property Measurement System (PPMS) with ACMSII option and the J_c was determined using the Bean model [21]. Similarly, the structural properties were determined using x-ray diffraction (XRD) on Panalytical Empyrean with Cu Kα radiation.

The samples were then subjected to Ag^+ ion irradiation at the Australian National University Heavy Ion Acceleration Facility using energies of 75 MeV and 150 MeV and fluences varying between 2–8·10^{11} ions/cm^2, as previously done in [22]. Hereafter, the samples are named 2e11, 4e11, 6e11, and 8e11, with the energy always written out explicitly. After irradiation, the superconducting and structural properties were re-evaluated using the same methods as before irradiation. During the irradiation, the samples were masked and therefore only partially subjected to irradiation. Especially in samples 150 MeV 4e11 and 6e11 and 75 MeV series this shows up as a secondary phase in the XRD measurements and also in the T_c measurements. It does not significantly affect the J_c measurements, since the pinning by the irradiation tracks dominates.

Finally, the samples were patterned with wet chemical etching, and the angular dependence of the J_c was measured using the PPMS AC transport-option. After etching atomic force microscopy was used to determine the thickness, which was 235 $\pm$ 10nm for all samples. In order to determine the microstructure, two samples were measured with high-resolution transmission electron microscopy (HRTEM) using a JEOL JEM-2200FS electron microscope equipped with a 200 kV field emission gun (FEG). Additionally, a probe-corrected scanning transmission electron microscope (STEM) utilizing high-angle annular dark-field imaging (HAADF STEM) was employed using a Titan 80–300 microscope operating at a voltage of 200 kV.

III. Results and Discussion

A. Structural Results

In the XRD measurements prior to irradiation, all the films were found to be perfectly c-oriented (from texture scans), impurity-free (from $2\theta - \omega$ scans), well oxygenated (from the intensity ratio of (005)/(004) peaks [23]), and having the normal twin structure of an APC-free YBCO film (from $2\theta - \phi$ scans of the (122)/(212) peak set [24]). Williamson-Hall analysis [25] showed small residual microstrain.

After irradiation, it was observed that some of the films had two phases, as seen from Fig. 1(a) due to masking and alignment issues in the experiment. These phases were analyzed separately. The (005) peak of the irradiated phase, Phase 1, clearly and almost linearly moves to the left with increasing fluence, indicating an increase in the lattice parameter c, as seen in the top panel of Fig. 1(b). This occurs with both irradiation energies used. As seen from the intensity ratios of the (005)/(004) peaks and the Williamson-Hall microstrain (Fig. 1(b)), this is not due to changes in the overall oxygenation level of the samples nor the increase of microstrain (with the exception of the 8e11 samples). Rather, we believe it is due to uniform strain caused by the introduction of the amorphous irradiation tracks.

The STEM images shown in Fig. 2 verify this interpretation. Irradiation forms very straight tracks through the sample

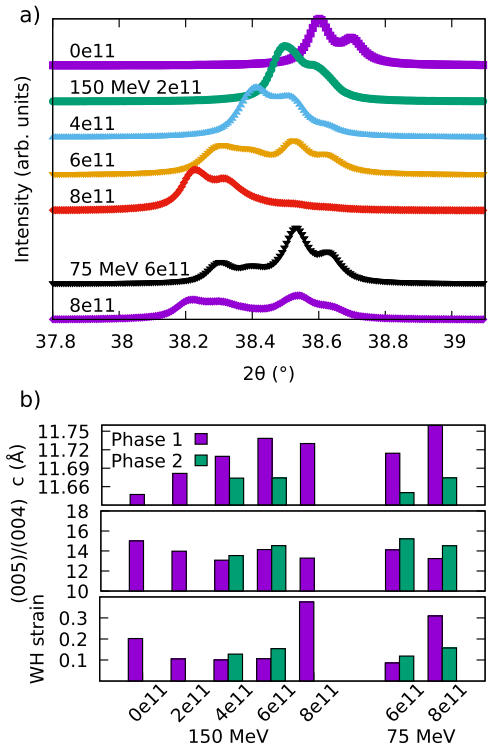

Fig. 1. a) The XRD scans of the (005) peaks of the samples, where the double peak structure, e.g. in 0e11, comes from the Cu Kα_1/Kα_2 radiation from the x-ray tube. Phase 1 is the irradiated phase and Phase 2 the masked parts. The 0e11 sample is shown as part of the Phase 1 for clarity. b) The calculated c lattice parameters, intensity ratios of (005)/(004) peaks, and the Williamson-Hall (WH) microstrains for the irradiated samples. The two phases were analyzed separately.

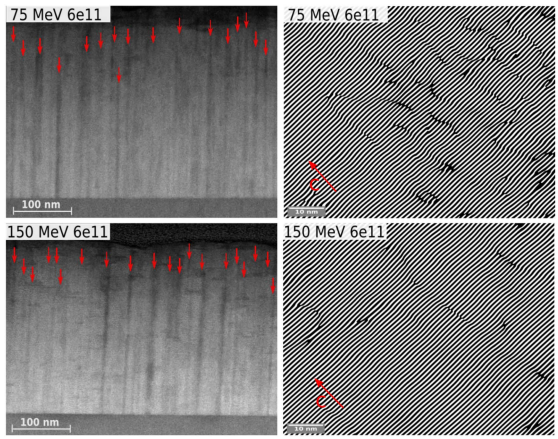

Fig. 2. STEM images of the irradiation tracks in the 6e11 samples irradiated with ions having energies of 75 MeV and 150 MeV. The right panels show inverse FFT-images of higher magnification highlighting the difference in the number of defects between the energies.

where the crystal structure is distorted. Between the tracks the crystal structure remains similar to the non-irradiated samples. The 150 MeV irradiation produces more continuous, film-penetrating tracks, while the 75 MeV irradiation causes more irregular distortion in the YBCO matrix, as shown on the right in Fig. 2, consistent with previous findings [26]. The track diameter

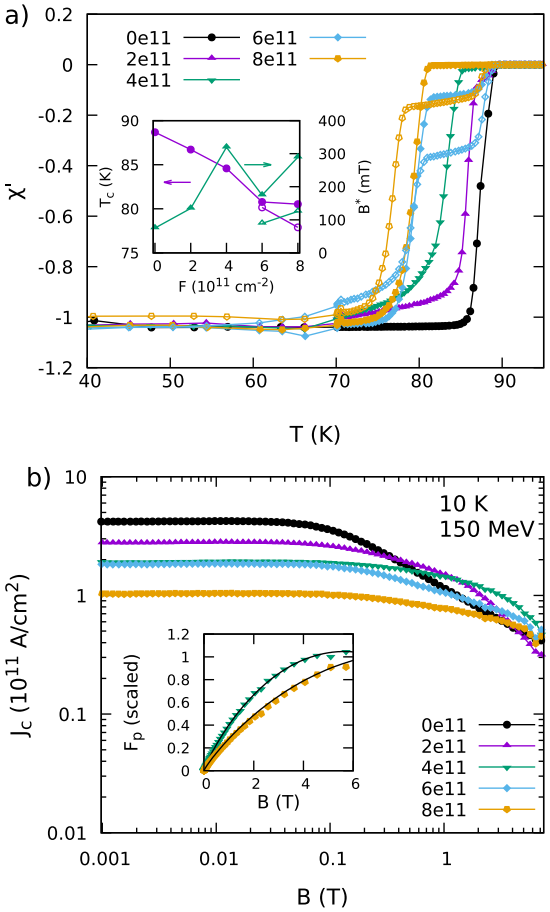

Fig. 3. a) Temperature dependence of susceptibility for the samples. The inset shows the fluence dependence of T_c with open symbols for the 75 MeV samples (left scale) and B^* determined as the field where $J_c = 0.9\, J_{c0}$ for all the samples (right scale). b) The magnetically measured field dependence of critical current density for the 150 MeV samples. The inset shows examples of the fitting to (1) for the 150 MeV samples 4e11 and 8e11.

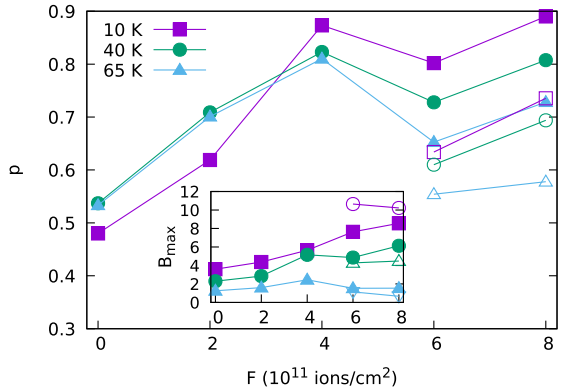

Fig. 4. Pinning parameter p, determined from the Dew-Hughes analysis, as a function of irradiation fluence and temperature. The inset shows the dependence of B_{max}. 150 MeV samples are shown with closed and 75MeV samples with open symbols.

was estimated from TEM images by identifying their edges, though this was challenging due to the gradual transition from amorphous to crystalline regions. Using this method, the average diameter was determined to be around 5 ± 1nm.

B. Superconducting Properties

As shown in Fig. 3(a) the irradiation has a clear effect on the critical temperature of the samples. T_c clearly decreases with the irradiation fluence, and smaller irradiation energy leads to a larger decrease in T_c. On the other hand, the width of the transition, ΔT_c, does not change significantly with the used fluence and there is no correlation between them. The samples that showed clear double peaks in XRD also show a step structure in the $\chi'(T)$ due to masking.

The magnetic field dependence of the critical current density, $J_c(B)$, is shown in Fig. 3(b) for the 150 MeV samples. As expected, the shape of the $J_c(B)$ curve changes with irradiation. Overall, the accommodation field, B^*, where the $J_c(B)$ curve starts decreasing, increases with fluence (inset of Fig. 3(b)), with the smaller value of the 6e11 sample attributed to the large portion of non-irradiated material in the sample. Without detailed analysis, it is clearly seen that the degradation of J_c with field decreases with increasing irradiation fluence.

We used the Dew-Hughes [27], [28] equation

$$F_p/F_{p,max} \propto (B/B_{max})^p (1 - B/B_{max})^q, \quad (1)$$

where $F_p = J_c B$ is the pinning force, p and q are exponents that describe the field dependence, and $F_{p,max}$ and $B_{max} = B_{irr}\frac{p}{p+q}$ [28] are parameters, which are used to scale the $F_p(B)$ before the fitting of p. Using $q = 1.1$ [28], we obtained the values shown in Fig. 4. Overall, with increasing irradiation fluence, p changes from 0.5, which is typical for samples with mostly natural defects (e.g., dislocations and twins), to 0.9, which is typical for samples with strong pinning sites, such as nanorods. Higher energy irradiation increases p more than lower energy, indicating stronger pinning, which is consistent with the results from TEM.

The absolute value of $F_{p,max}$ was found to be approximately the same for all the samples, indicating that the pinning sites have similar pinning force. On the other hand, B_{max} increases with fluence but decreases with temperature (Fig. 4 inset). B_{max} is expected to depend on the pinning site radius, r_r, and density, which in our case is the fluence, F. Clearly, $F \propto 1/d_r^2$, where d_r is the average distance between the pinning sites, as given by [7]

$$B_{max} \propto (r_r F)^{1/3}, \quad (2)$$

this behavior is to be expected.

Since irradiation forms strictly c-axis aligned tracks, as can be seen from the TEM (Fig. 2), the angular dependence of J_c also shows very narrow peaks at $B \parallel c$, as illustrated in Fig. 5 for all the samples at 8 T and 10 K. Additionally, the natural anisotropy a-peaks are observed. It is evident that at 150 MeV with at low fluence, i.e. large distance between the pinning sites, the c-peaks are narrower and higher. This is because, at high fluences, vortices can bend from one pinning site to a neighboring one, whereas at small fluences, it is energetically favorable for vortices to follow the track throughout the sample.

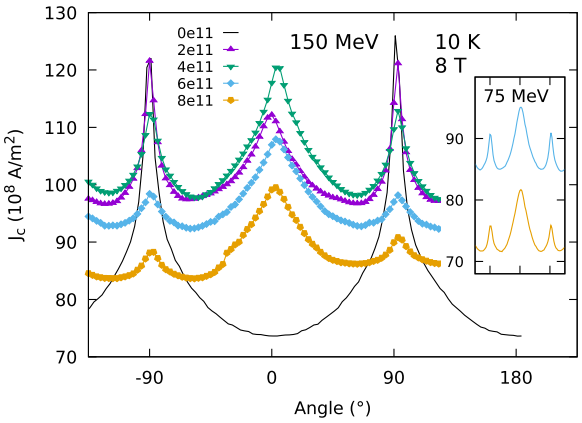

Fig. 5. Angular dependence of J_c for all the samples at 8 T and 10 K. The black line is a reference non-irradiated sample. The inset shows the samples irradiated at 75 MeV. The YBCO c-axis is at 0°.

TABLE I
THE OBSERVED REDUCTION IN J_c AT 10K FOR THE 150 MEV SAMPLES, ALONG WITH THE CALCULATED EFFECTIVE DIAMETER OF THE RODS, $2r_{EFF}$, THE DISTANCE BETWEEN THE ROD CENTERS, D_r, THE AVERAGE FREE YBCO MATRIX SPACE BETWEEN THE RODS, D_{FREE}, AND THE CALCULATED MATCHING FIELD, B_ϕ

F (10^{11} ions/cm^2)	J_c'(0)/J_c(0)	$2r_{eff}$ (nm)	D_r (nm)	D_{free} (nm)	B_ϕ (T)
2	0.89	8.18	22	14.2	4.1
4	0.77	8.47	16	7.3	8.3
6	0.72	7.7	13	5.2	12.4
8	0.65	7.45	11	3.7	16.6

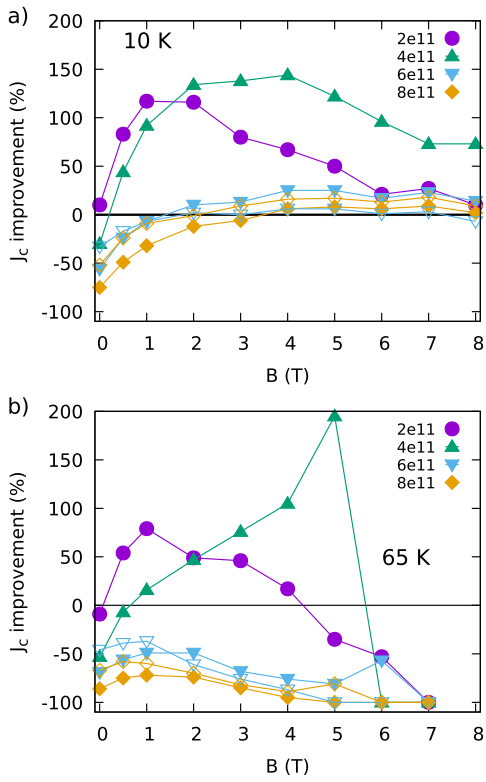

Fig. 6. Improvement of $J_c(B||c)$ as (J_c(0)-J_c'(0))/J_c(0) with irradiation at 10K (a) and at 65K (b) compared to the same sample before irradiation. 15 0MeV samples are shown with closed and 75MeV samples with open symbols.

Since the tracks are discontinuous at 75 MeV irradiation, a similar widening with fluence is not observed.

Comparing the $J_c(B)$ values of the irradiated samples to the $J_c(B)$ values of the same sample prior to irradiation, it is evident that irradiation decreases the absolute J_{c0} (see Table I), similarly to observations made for samples with APCs; J_{c0} decreases with the number of pinning sites. The simplest explanation for this is that the pinning sites are no longer superconductors, and therefore the superconducting volume of the sample decreases.

However, in a magnetic field, J_c increases significantly, especially at high temperature for the 4e11 sample (Fig. 6). It is evident that the 4e11 sample shows the highest increase at both low and high temperatures, although all samples exhibit smaller improvements at higher temperatures. With a smaller fluence than $4 \cdot 10^{11}$ ions/cm^2, there is an improvement in J_c with field, but the maximum is achieved at a lower field, and at higher fluences, the decrease in J_{c0} is not fully compensated by the improved pinning. The field of maximum J_c increases with fluence, as also seen from the F_p fittings. As shown in the insets of Fig. 6, for lower energy irradiation, the observed improvement in J_c is less significant and remains negative at 65 K. This is due to the easier movement of vortices with non-continuous tracks.

In order to better understand the results in Fig. 6, we can calculate the optimal distance between the ion tracks and compare it to the theoretical models [4], [8] for the 150 MeV samples where the tracks are continuous through the film and a maximum in J_c improvement is found. Assuming that the YBCO matrix remains in its original form, as indicated by the XRD results (Fig. 1), and that the reduction in J_{c0} is due to the loss of superconducting volume, we can express the expected loss in J_c as

$$\frac{J_c(0)'}{J_c(0)} \propto 1 - F\pi r_{eff}^2, \tag{3}$$

where $J_c(0)'$ is the J_c after irradiation, F is the irradiation fluence and r_{eff} is the theoretical rod radius needed to decrease the J_c by the observed amount. By observing the decrease in J_{c0}, we can calculate the effective rod radii, which are shown in Table I. The fact that we obtain almost identical values (7.5–8.5 nm diameter) for all samples without any fitting is promising. This is slightly larger than the value observed in TEM, probably indicating a thin dead layer around the amorphous core. From the fluence, we calculate the distance between the rod centers, denoted as D_r in the table, as well as the free YBCO matrix space between the outer edges of the rods (D_{free}). Additionally, we have calculated the matching field, B_ϕ, from the fluence. This naturally increases with fluence, but also closely matches the dependence of B_{max} shown in Fig. 4 and given by (2).

Theoretical models [4], [8] predict that the optimal free distance between the nanorods should be equal to the diameter of the rods. From Table I, it is evident that for this set of samples, the models align well with the experimental results. The 4e11 sample is closest to this value and shows the highest in-field improvement in J_c. In contrast, the 2e11 sample has rods that are too far apart, while the higher fluence samples have rods that are

too close, which significantly diminishes the superconducting volume. This is consistent with the J_c results shown in Fig. 6, where the high-fluence samples exhibit minimal improvement in J_c.

IV. Conclusion

To verify the theoretical predictions that optimal J_c in high-temperature superconductors is achieved when the diameter of the nanorod pinning sites equals the free superconducting matrix distance between them, we used APC-free YBCO films and irradiated them with Ag^+ ions. The samples were then examined for their structural and superconducting properties.

It was observed that the ion tracks were all parallel to the c -axis of the sample. Tracks formed with 150 MeV ions were continuous and measured about 5nm in diameter, whereas those formed with 75 MeV ions were more discontinuous. The results were in line with previous experiments [18], [22], [26].Both T_c and J_{c0} decreased with irradiation, but J_c in the magnetic field increased. The maximum increase was observed with the sample irradiated with 150 MeV ions at $4 \cdot 10^{11}$ ions/cm^2 fluence, where the distance between the rods was closest to the diameter of the rods. Thus, the models are experimentally validated for these very pure samples, which contain no other strong extrinsic pinning sites.

Acknowledgment

The authors acknowledge access to the Heavy-Ion Accelerator Facility funded under the National Collaborative Research Infrastructure Strategy (NCRIS), Australia.

References

[1] A. C. Wulff, A. B. Abrahamsen, and A. Insinga, "Topical Review: Multifilamentary coated conductors for ultra-high magnetic field applications," *Supercond. Sci. Technol.*, vol. 34, 2021, Art. no. 053003.

[2] J. MacManus-Driscoll and S. Wimbush, "Processing and application of high-temperature superconducting coated conductors," *Nat. Rev. Mater.*, vol. 6, 2021, Art. no. 587.

[3] T. J. Haugan, T. Puig, K. Matsumoto, and J. Wu, "Artificial pinning centers in (Y,RE)-Ba-Cu-O superconductors: Recent progress and future perspective," *Supercond. Sci. Technol.*, vol. 33, 2019, Art. no. 040301.

[4] P. Paturi and H. Huhtinen, "Roles of electron mean free path and flux pinning in optimizing the critical current in YBCO superconductors," *Supercond. Sci. Technol.*, vol. 35, 2022, Art. no. 065007.

[5] E. F. Talantsev and J. L. Tallon, "Universal self-field critical current for thin-film superconductors," *Nat. Commun.*, vol. 6, 2015, Art. no. 7820.

[6] E. F. Talantsev, W. P. Crump, and J. L. Tallon, "Universal scaling of the self-field critical current in superconductors: From sub-nanometre to millimetre size," *Sci. Rep.*, vol. 7, 2017, Art. no. 10010.

[7] T. Matsushita, *Flux Pinning in Superconductors*. Berlin, Germany: Springer, 2007.

[8] E. Rivasto, M. Todorovic, H. Huhtinen, and P. Paturi, "Optimization of high-temperature superconducting multilayer films using artificial intelligence," *New J. Phys.*, vol. 25, 2023, Art. no. 113046.

[9] G. Blatter, M. V. Feigel'man, V. B. Geshkenbein, A. I. Larkin, and V. M. Vinokur, "Vortices in high-temperature superconductors," *Rev. Modern Phys.*, vol. 66, pp. 1125–1388, 1994.

[10] H. Palonen, J. Jäykkä, and P. Paturi, "Modeling reduced field dependence of critical current density in $YBa_2Cu_3O_{6+x}$ films with nanorods," *Phys. Rev. B*, vol. 85, 2012, Art. no. 024510.

[11] M. M. Aye, M. Z. Khan, E. Rivasto, J. Tikkanen, H. Huhtinen, and P. Paturi, "Role of columnar defect size in angular dependent flux pinning properties of YBCO thin films," *IEEE Trans. Appl. Supercond.*, vol. 29, no. 5, Aug. 2019, Art. no. 8000805.

[12] B. Maiorov et al., "Synergetic combination of different types of defect to optimize pinning landscape using $BaZrO_3$-doped $YBa_2Cu_3O_7$," *Nat. Mater.*, vol. 8, pp. 398–404, 2009.

[13] V. Ogunjimi et al., "Enhancing magnetic pinning by $BaZrO_3$ nanorods forming coherent interface by strain-directed ca-doping in $YBa_2Cu_3O_{7-x}$ nanocomposite films," *Supercond. Sci. Technol.*, vol. 34, 2021, Art. no. 104002.

[14] A. V. Ovcharov et al., "Microstructure and superconducting properties of high-rate PLD-derived $GdBa_2Cu_3O_{7-\delta}$ coated conductors with $BaSnO_3$ and $BaZrO_3$ pinning centers," *Sci. Rep.*, vol. 9, no. 1, 2019, Art. no. 15235.

[15] B. Gautam et al., "Probing the effect of interface on vortex pinning effiency of one-dimensional $BaZrO_3$ and $BaHfO_3$ artificial pinning centers in YBa_2 Cu_3O_{7+x} thin films," *Appl. Phys. Lett.*, vol. 113, 2018, Art. no. 212602.

[16] J. Wu and J. Shi, "Interactive modeling-synthesis- characterization approach towards controllable in situ self-assembly of artificial pinning centers in RE-123 films," *Supercond. Sci. Technol.*, vol. 30, 2017, Art. no. 103002.

[17] T. Horide, "Structural evolution induced by interfacial lattice mismatch in self-organized $YBa_2Cu_3O_{7-\delta}$ nanocomposite film," *ACS Nano*, vol. 11, pp. 1780–1788, 2017.

[18] T. Sueyoshi, "Modification od critical current density anisotropy in high-T_c superconductors by using heavy-ion irradiations," *Quantum Beam Sci.*, vol. 5, 2021, Art. no. 16.

[19] M. Z. Khan et al., "Strongly enhanced growth of high-temperature superconducting films on an advanced metallic template," *Cryst. Growth Des.*, vol. 22, pp. 2097–2104, 2022.

[20] M. M. Aye, E. Rivasto, H. Huhtinen, and P. Paturi, "Enhanced critical current density in heterostructural YBCO/Ca-doped YBCO multilayers," *Cryst. Growth Des.*, vol. 24, pp. 4545–4555, 2024.

[21] H. P. Wiesinger, F. M. Sauerzopf, and H. W. Weber, "On the calculation of J_c from magnetization measurements on superconductors," *Physica C*, vol. 203, pp. 121–128, 1992.

[22] N. M. Strickland et al., "Isotropic and anisotropic flux pinning induced by heavy-ion irradiation," *IEEE Trans. Appl. Supercond.*, vol. 32, no. 4, Jun. 2022, Art. no. 8000505.

[23] J. Ye and K. Nakamura, "Quantitative structure analyses of YBCO thin films: Determination of oxygen content from X-ray-diffraction patterns," *Phys. Rev. B*, vol. 48, pp. 7554–7564, 1993.

[24] P. Paturi, M. Peurla, K. Nilsson, and J. Raittila, "Crystalline orientation and twin formation in YBCO thin films laser ablated from a nanocrystalline target," *Supercond. Sci. Technol.*, vol. 17, pp. 564–570, 2004.

[25] B. Himabindu, N. L. Devi, and B. R. Kanth, "Microstructural parameters from X-ray peak profile analysis by Williamson-Hall models; a review," *Mater. Today: Proc.*, vol. 47, pp. 4891–4896, 2021.

[26] M. Toulemonde, S. Bouffard, and F. Studer, "Swift heavy ions in insulating and conducting oxides: Tracks and physical properties," *Nucl. Instrum. Meth. Phys. Res. B*, vol. 91, 1994, Art. no. 108.

[27] D. Dew-Hughes, "Flux pinning mechanisms in type II superconductors," *Philos. Mag.*, vol. 30, 1974, Art. no. 293.

[28] P. Paturi, M. Malmivirta, H. Palonen, and H. Huhtinen, "Dopant diameter dependence of $J_c(B)$ in doped YBCO films," *IEEE Trans. Appl. Supercond.*, vol. 26, no. 3, Apr. 2016, Art. no. 8000705.